Electronic Supplementary Material (ESI) for Journal of Materials Chemistry C.
This journal is © The Royal Society of Chemistry 2021

Supporting Information

Conductivity and Memristive Behavior of Completely Charged Domain Walls in Reduced Bidomain Lithium Niobate

Ilya V. Kubasov, Aleksandr M. Kislyuk, Tatiana S. Ilina, Andrey S. Shportenko, Dmitry A. Kiselev, Andrei V. Turutin, Aleksandr A. Temirov, Mikhail D. Malinkovich, Yuriy N. Parkhomenko*

Supporting Information S1

OHHMIC BEHAVIOR OF Cr|$LiNbO_3$ ELECTRODE

Selection of chromium as the material for the bottom electrode was dictated by the fact that the contact between chromium and LN behaves ohmic[1]. However, as the previous results were obtained with non-reduced LN, we additionally tested the contact by recording the I-V curves for the additional RLN single domain sample. The measurements were provided for samples with different reduction levels (were controlled by changing the time of the reduction annealing). The sketch of the circuit for measurements of I-V curves with full face electrodes is shown in Figure S1.1 (a). The measured data are shown in Figure S1.1 (b) confirmed the ohmic behavior of the contact Cr|RLN with the electrical conductivity of ca. $8 \cdot 10^{-10}\ \Omega^{-1}cm^{-1}$. We did not found any significant time-dependent current through the sample at any voltage in the investigating range (including 0 V) which indicates the absence of electrochemical interaction between RLN and Cr.

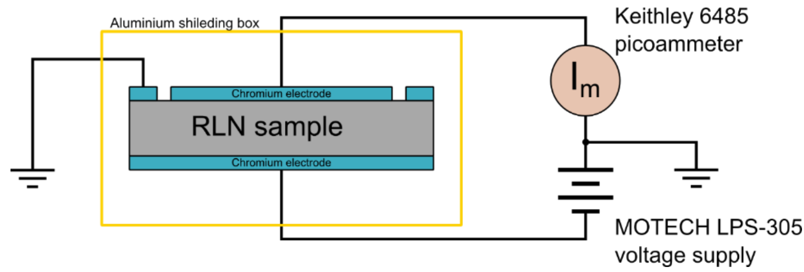

a

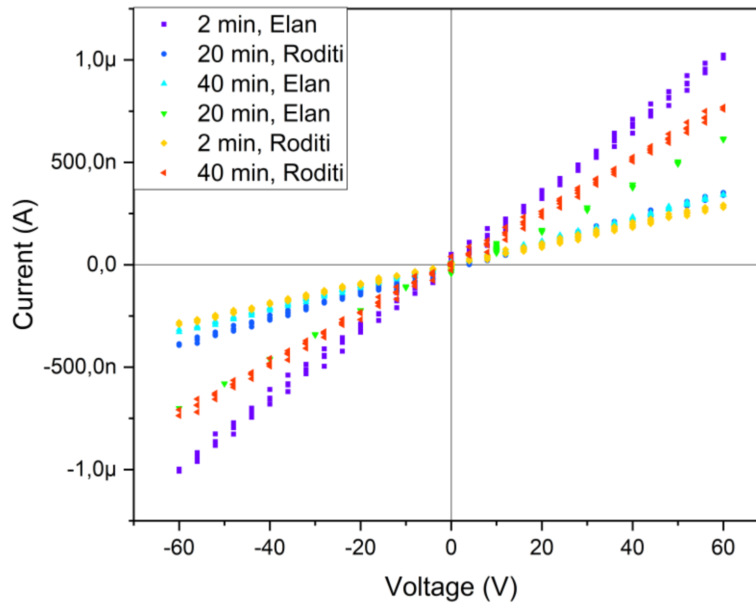

b

Figure S1.1. (a) schematic presentation of a circuit for measurement of I-V curves of Cr|RLN|Cr samples; (b) Family of I-V curves registered on several Cr|RLN|Cr samples; time in the legend indicates a duration of reducing annealing, name corresponds to a supplier of the LN crystals (Elan Optics Ltd, Russia and The Roditi International Corporation Ltd, United Kingdom)

To study the domain structure and conductive state of the domain wall as well as the single domain regions of the bidomain crystals we used conventional lateral PFM (LPFM) and c-AFM techniques. The investigations were performed on an MFP-3D Stand-Alone AFM (Asylum Research). As x direction is non-polar in LN and the crystals were bonded to the metal plate, there were no pyroelectric currents during at temperatures lower 70°C (artifacts in c-AFM scans having likely the pyroelectric origin can be observed at elevated temperature and described in the manuscript). All AFM scans were done with the cantilever moving along the z-axes of the specimens.

The material of the tip coating could also influence the results of I-V measurements, thus we compared two different types of probes: a brand-new commercial Pt-coated NSG10/Pt cantilever and re-coated with a 30 nm thick Cr film NSG10/Pt cantilever. The results of the comparison are given in Figure S1.2. We did not observe any significant difference between the I-V curves, the slight discrepancies near zero voltage are most likely due to non-ideal positioning of the probe on the CDW and lower quality of home-made Cr coating comparatively to industrial quality of Pt coating. Therefore only Pt-coated probes were used hereinafter (it is worth noting that there is evidence of ohmic behavior of Pt|RLN contacts[2]; however, in the mentioned study paint electrodes were used, thus their results cannot be fully comparable with ours).

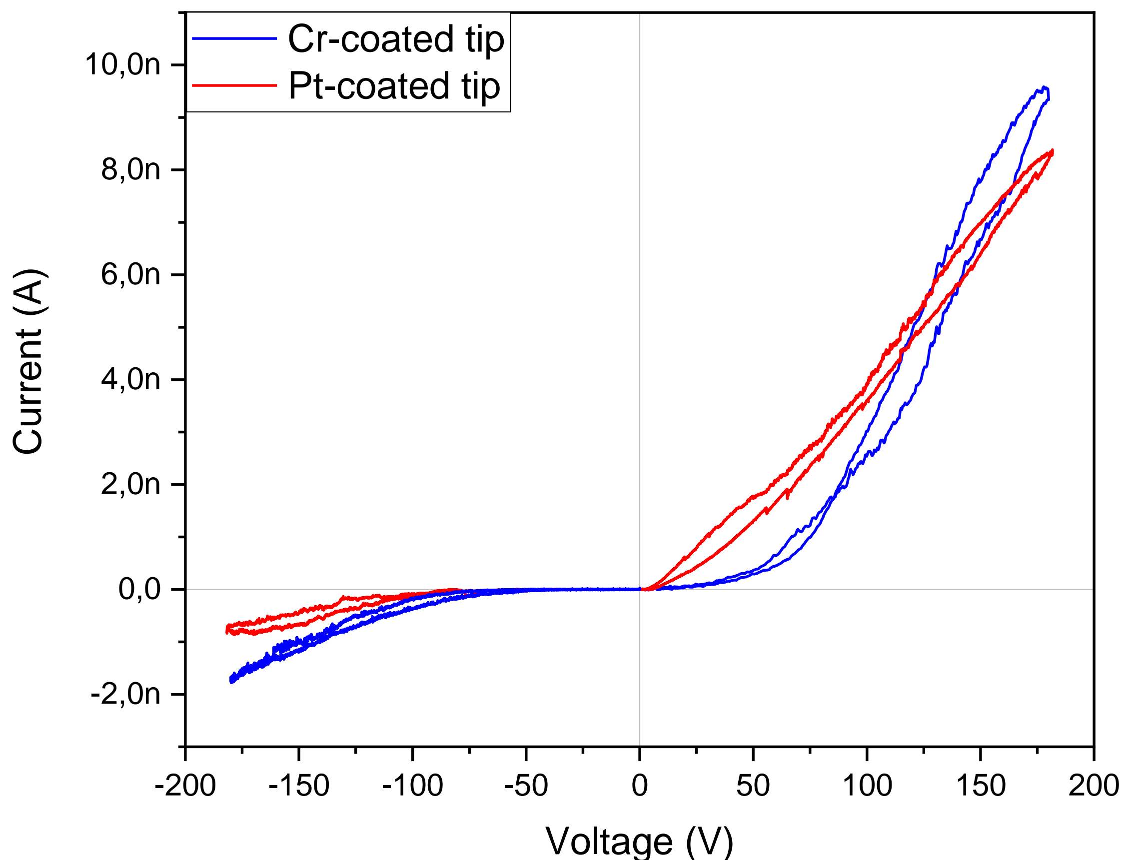

Figure S1.2. Comparison of I-V curves obtained at the H-H domain wall with Cr and Pt tip coatings (the curves were registered in different points of sample)

Supporting Information S2

DETAILS OF REGISTRATION OF THE I-V CURVES

Recently, it was shown by Kelvin probe force microscopy that the width of the area around the CDW in RLN where surface electrical potential differs from a single domain can reach 2 μm[3]. Therefore, the distance between the points corresponding to “current in a single domain region far from the CDW” and the CDW itself was at least 5 μm. We additionally registered I-V curves in the single domain regions at the distance of several dozens of μm left and right from the CDWs in each of the RLN samples found no difference between both I-V curves (Figure S2.1, Figure S2.2) and shapes of the induced domains (Figure S2.3). Thus, for clarity, we give here figures with all these six measuring points shown in one scan.

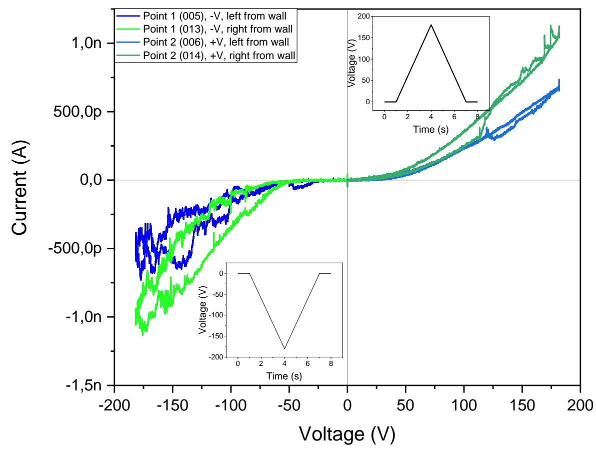

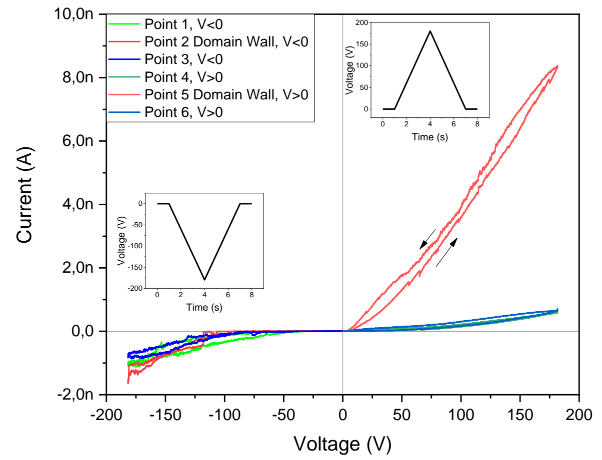

a

b

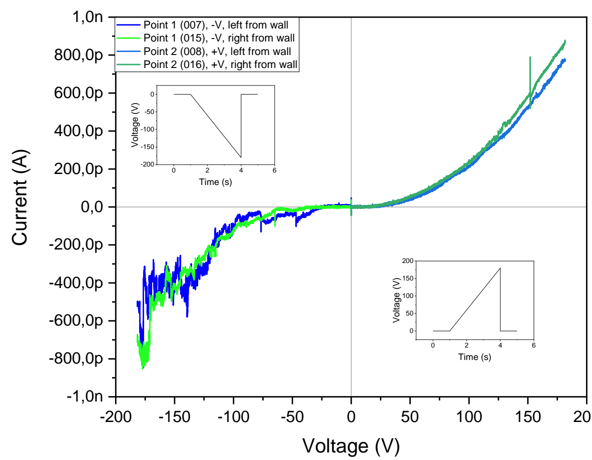

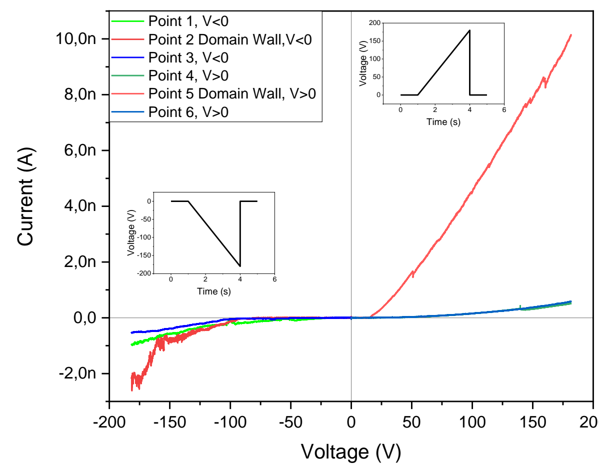

c

d

Figure S2.1. I-V curves measured in single domain regions (a), (c) and in the vicinity of the H-H CDW by triangle (a), (b) and sawtooth (c), (d) signals

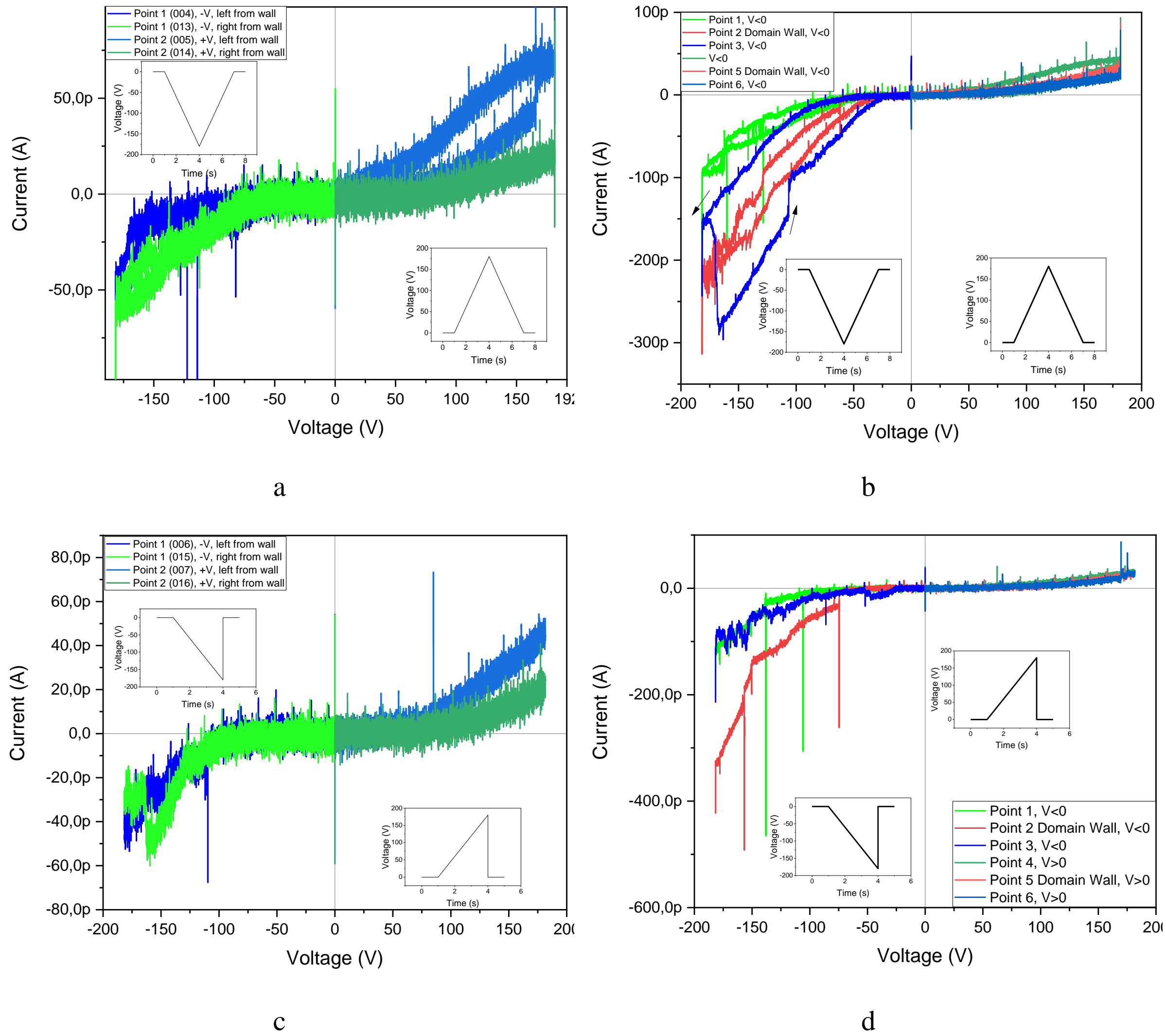

Figure S2.2. I-V curves measured in single domain regions (a), (c) and in the vicinity of the T-T CDW by triangle (a), (b) and sawtooth (c), (d) signals

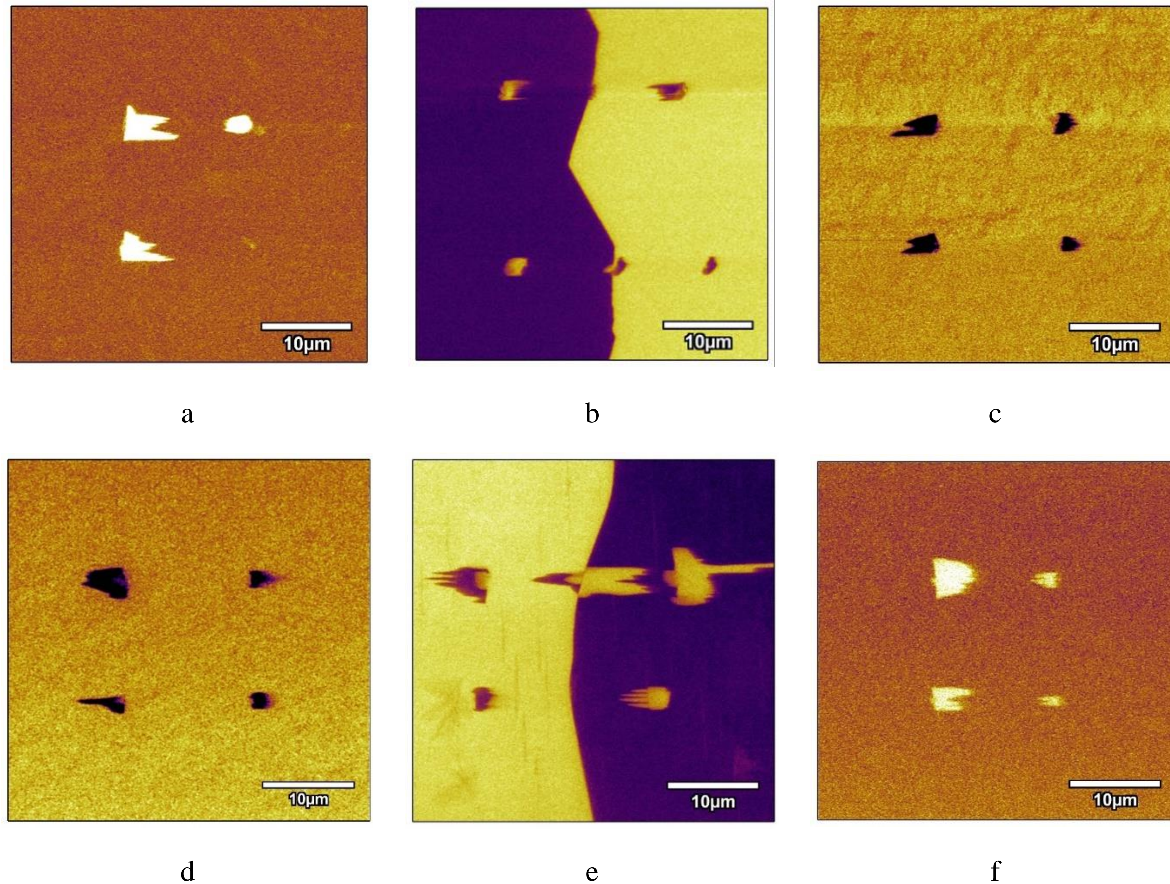

Figure S2.3. Domains reversed left (a), (d) and right (c), (f) from the CDWs as well as in the vicinity of the wall (b), (e) by measuring I-V curves. In scans (a), (c), (d), (f) left points correspond to negative tip bias voltage, right points correspond to positive voltage, upper points are reversed by triangle wave while bottom points are reversed by the sawtooth wave. Details about the reversal of scans (b), (e) can be found in the manuscript as well as in Figure 1

Sawtooth and triangle bias waveforms with a magnitude up to ±180 V were compared. The first one allows registration of simple I-V curve when the second one helps to estimate possible hysteretic change of conductivity as the result of the local ferroelectric domain reversal. We intentionally did not register I-V curves with pulsed or square bias waveforms (notwithstanding they are widely used in CDW studies, see e.g. Refs. 4,5) because at the first stage of the study it was revealed that signals having short rise or fall times cause strong current oscillations possibly related to a finite inductivity and capacitance of the measuring system. These oscillations repeated and had almost the same amplitudes in both samples as well as in non-piezoelectric glass slide used as reference (Figure S2.4)

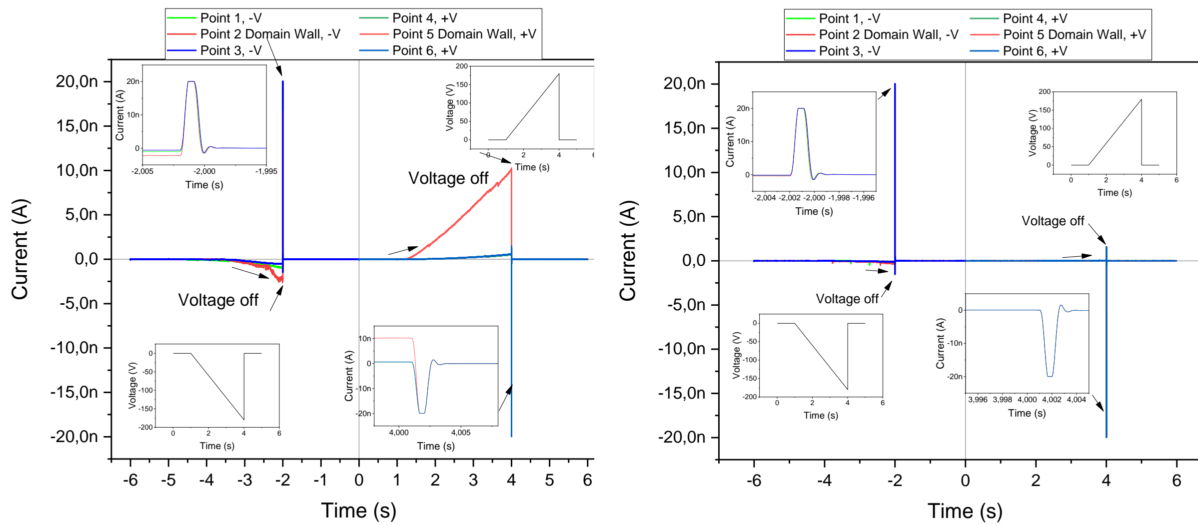

a b

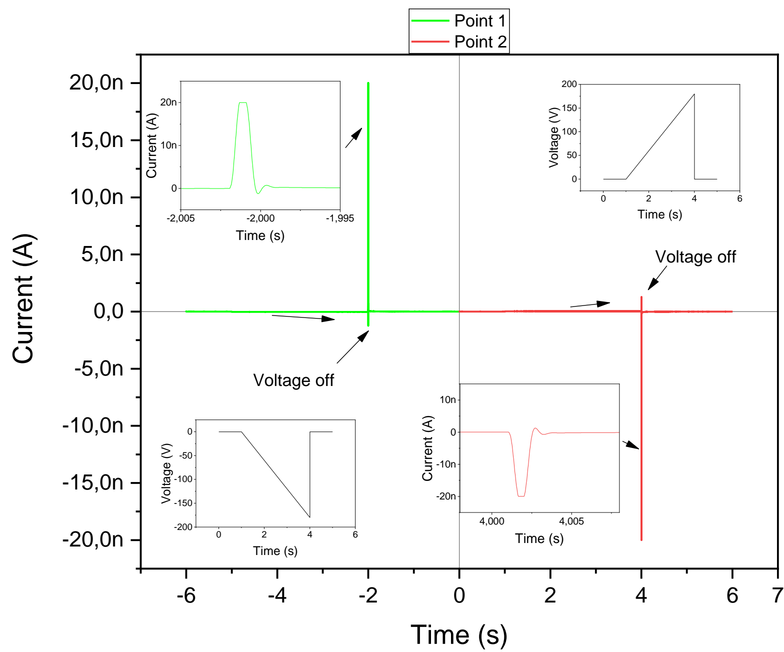

c

Figure S2.4. Current vs time characteristics illustrating current oscillations caused by a short rise or fall times measured in the proximity of the H-H (a), T-T (b) CDWs as well as on glass (c)

Supporting Information S3

POLARIZATION OF T-T CDW BY C-AFM SCANNING

In the c-AFM scans measured with low tip bias voltage the T-T CDW was never observed. However, the increase of bias tip voltage in c-AFM scanning up to |-30 V| led to the appearance of the T-T CDW in the scans as a slight trace of enhanced current. After registration of the surface current distribution PFM scan of a larger area in the same place showed slight polarization of the square-shaped domain coincident with the area of c-AFM scan (Figure S3).

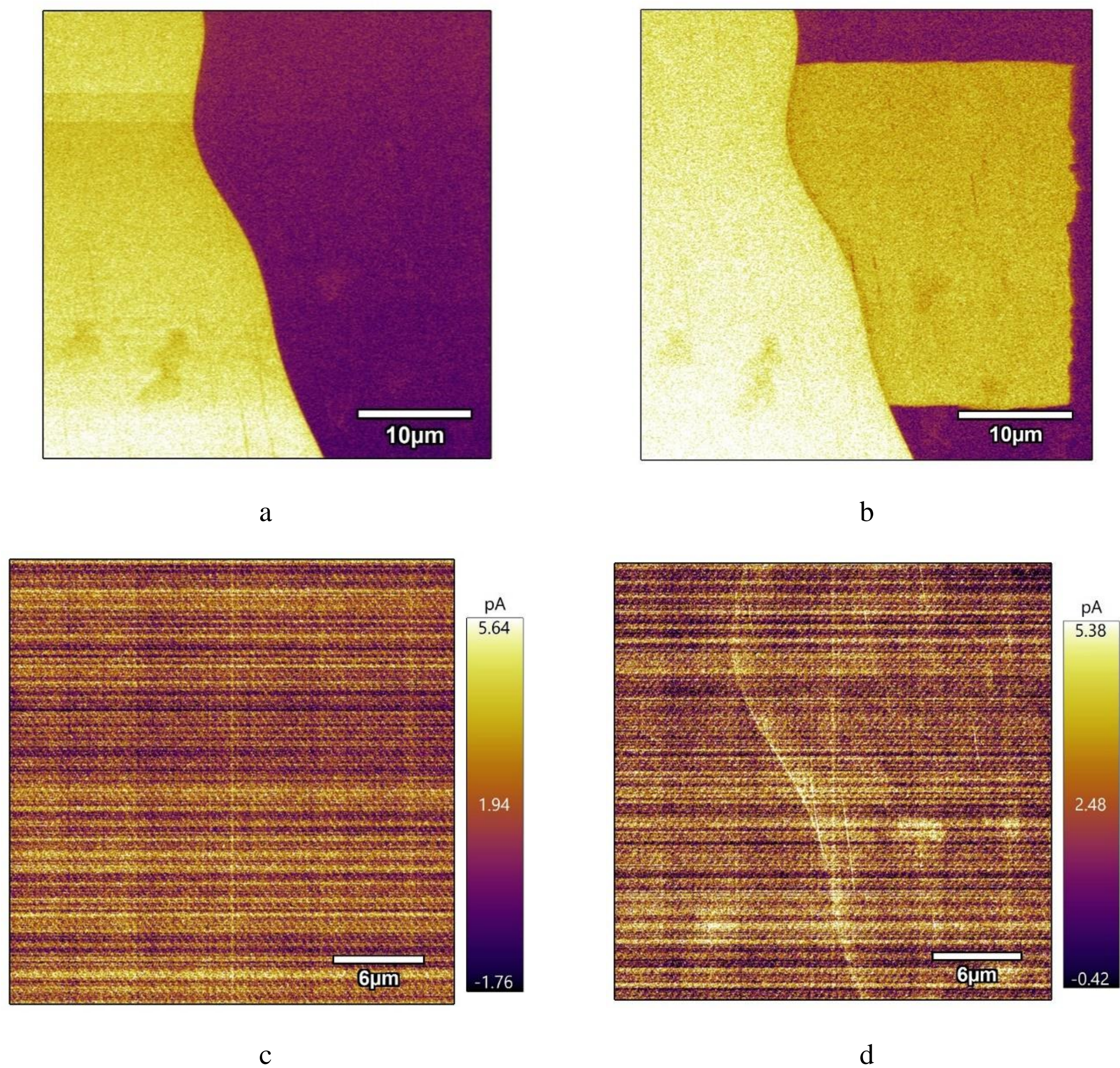

Figure S3. PFM scans of the proximity of the T-T CDW obtained before (a) and after (b) c-AFM measurement with bias tip voltage of -30 V; c-AFM scans of the same CDW obtained with bias tip voltage of -7 V (c) and -30 V (d)

Supporting Information S4

An integrated circuit with a high density of CDW-based devices can be produced basing on a conventional z-cut LN wafer with a bidomain structure where the boundary is underlaying in several μm's from the surface. In order to provide contacts to CDW different types of patterned etching can be utilized, fortunately negative surface of an H-H bidomain plate is rapidly etched in HF[6]. Selecting appropriate electrode material and size one can change the type of conductivity in the region between the contacts as well as tune the resistance of the CDW. Moreover, several contacts can be applied to one region of the CDW and play the roles of axons in a neuromorphic cell. Also, extra memristive channels from the surface to the H-H CDW can be produced by domain reversal with the application of an external voltage. Schematic representation of a possible concept of such an integrated circuit is shown in Figure S4.

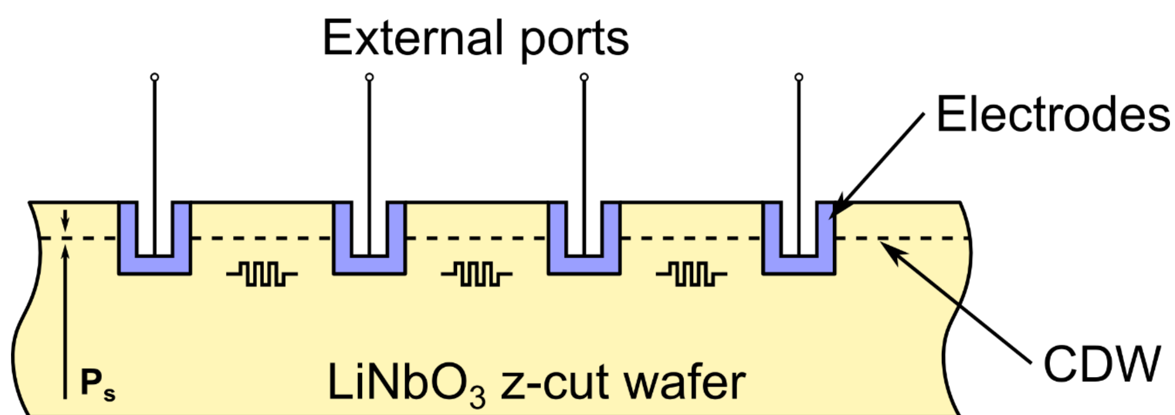

Figure S4. Schematic representation of a possible concept of an integrated circuit with high density of CDW-based devices on a conventional z-cut wafer

REFERENCES

1 M. Schröder, A. Haußmann, A. Thiessen, E. Soergel, T. Woike and L. M. Eng, *Adv. Funct. Mater.*, 2012, **22**, 3936–3944.

2 A. Dhar, N. Singh, R. K. Singh and R. Singh, *J. Phys. Chem. Solids*, 2013, **74**, 146–151.

3 A. M. Kislyuk, T. S. Ilina, I. V. Kubasov, D. A. Kiselev, A. A. Temirov, A. V. Turutin, M. D. Malinkovich, A. A. Polisan and Y. N. Parkhomenko, *Mod. Electron. Mater.*, 2019, **5**, 51–60.

4 P. Maksymovych, J. Seidel, Y. H. Chu, P. Wu, A. P. Baddorf, L.-Q. Chen, S. V. Kalinin and R. Ramesh, *Nano Lett.*, 2011, **11**, 1906–1912.

5 T. R. Volk, R. V. Gainutdinov and H. H. Zhang, *Appl. Phys. Lett.*, 2017, **110**, 132905.

6 K. Nassau, H. J. Levinstein and G. M. Loiacono, *Appl. Phys. Lett.*, 1965, **6**, 228–229.